Hyperpolarized ^{13}C dehydroascorbate as an endogenous redox sensor for in vivo metabolic imaging

Kayvan R. Keshari, John Kurhanewicz, Robert Bok, Peder E. Z. Larson, Daniel B. Vigneron, and David M. Wilson[1]

Department of Radiology and Biomedical Imaging, University of California San Francisco, 1700 4th Street, Byers Hall 203, San Francisco, CA 94158

Edited by Alexej Jerschow, New York University, New York, NY, and accepted by the Editorial Board September 14, 2011 (received for review May 2, 2011)

Reduction and oxidation (redox) chemistry is involved in both normal and abnormal cellular function, in processes as diverse as circadian rhythms and neurotransmission. Intracellular redox is maintained by coupled reactions involving NADPH, glutathione (GSH), and vitamin C, as well as their corresponding oxidized counterparts. In addition to functioning as enzyme cofactors, these reducing agents have a critical role in dealing with reactive oxygen species (ROS), the toxic products of oxidative metabolism seen as culprits in aging, neurodegenerative disease, and ischemia/ reperfusion injury. Despite this strong relationship between redox and human disease, methods to interrogate a redox pair in vivo are limited. Here we report the development of [1-^{13}C] dehydroascorbate [DHA], the oxidized form of Vitamin C, as an endogenous redox sensor for in vivo imaging using hyperpolarized ^{13}C spectroscopy. In murine models, hyperpolarized [1-^{13}C] DHA was rapidly converted to [1-^{13}C] vitamin C within the liver, kidneys, and brain, as well as within tumor in a transgenic prostate cancer mouse. This result is consistent with what has been previously described for the DHA/Vitamin C redox pair, and points to a role for hyperpolarized [1-^{13}C] DHA in characterizing the concentrations of key intracellular reducing agents, including GSH. More broadly, these findings suggest a prognostic role for this new redox sensor in determining vulnerability of both normal and abnormal tissues to ROS.

MRI | molecular imaging | probe | kinetics

Ascorbic acid (Vitamin C) is an essential cofactor in reactions catalyzed by Cu^{+}- dependent monooxygenases and Fe^{2+}-dependent dioxygenases, required for the enzymatic biosynthesis of collagen, catecholamines, and peptide neurohormones (1–3). Vitamin C is also an effective reducing agent protecting cells from the injurious effects of reactive oxygen species (4). Pauling championed the antiviral properties of Vitamin C, and cells of the immune system including mononuclear leukocytes and neutrophils are known to accumulate large quantities of ascorbate, which may be protective against free radicals generated during the respiratory burst (5–7). In reactions with free radicals, ascorbic acid acts as a stable electron donor, converted to the radical anion semidehydroascorbate, which can be recycled back to ascorbate by a number of mechanisms, or undergo disproportionation to form ascorbate and dehydroascorbate (8). Recently, a number of mechanisms have been elucidated for the two-electron reduction of dehydroascorbate (DHA) to Vitamin C in animals. This conversion can take place via a glutathione (GSH)- dependent mechanism catalyzed by glutaredoxin, protein disulfide isomerase, and glutathione transferases or by NADPH-dependent mechanisms including reduction catalyzed by 3α-hydroxysteroid dehydrogenase (9–12). In turn, GSH levels are maintained by the NADPH-dependent reduction of oxidized glutathione (GSSG) (13) (Fig. 1*A*). Redox reactions are broadly linked to processes both normal and pathologic, but have particular relevance to cancer with glutathione metabolism playing both protective and pathologic roles. Loss of the glutathione S-transferase M1 gene (GSTM1) correlates with increased susceptibility to lung and bladder cancer (14, 15), while elevated GSH in several tumors may confer resistance to chemo- and radiotherapy (16–18). These effects are thought to be secondary to cellular resistance to reactive oxygen species (ROS) including hydrogen peroxide and superoxide (19).

Although redox chemistry is a central feature of cellular processes, existing methods to interrogate coupled oxidation/reduction reactions in vivo have significant limitations, including poor tissue penetration (as is the case for optical probes) and prohibitively long scan times (20, 21). Here we describe a MR imaging agent, hyperpolarized [1-^{13}C] DHA, which is rapidly converted to [1-^{13}C] Vitamin C in vivo, at levels suitable for magnetic resonance spectroscopic imaging (MRSI) (Fig. 1*B*). DHA is maintained at much lower intracellular concentrations than Vitamin C, but has a number of unique properties that set it apart. While the Na^{+}- dependent cotransporters SVCT1 and SVCT2 transport Vitamin C, DHA is transported by facilitated diffusion via the glucose transporters GLUT1, GLUT2, and GLUT4, with rapid reduction of DHA to Vitamin C occurring within the cell (22). The transport, and structural properties of DHA make it an excellent candidate for in vivo metabolic studies using hyperpolarized ^{13}C MRSI. This new MRI technique to probe specific enzymatic pathways requires a labeled ^{13}C substrate with a long spin-lattice relaxation time (T_1), whose metabolic product is readily distinguishable by chemical shift (23–26). Recently, this technique has afforded modelling of rapid enzymatic fluxes in vivo, including the rapid conversion of [1-^{13}C] pyruvate to [1-^{13}C] lactate as mediated by lactate dehydrogenase (LDH) (27). In a similar vein, [1-^{13}C] DHA was designed to probe the kinetics of reduction in vivo, via GSH-mediated conversion to Vitamin C. Hyperpolarized [1-^{13}C] DHA was found to have a T_1 of 57 s at a clinically relevant field strength (3 T), and facile chemical reduction to [1-^{13}C] Vitamin C by $NaBH_3CN$ with a 3.8 ppm downfield chemical shift. In vivo, we observed rapid conversion to [1-^{13}C] Vitamin C in kidneys, liver, and tumor in a transgenic adenocarcinoma of the mouse prostate (TRAMP) model, as well as in a normal rat brain. These results highlight the utility of hyperpolarized [1-^{13}C] DHA as a probe for redox chemistry in living biologic systems, and provide evidence that GSH-mediated reduction of DHA is a feature of prostate cancer that may be exploited therapeutically.

Author contributions: K.R.K., J.K., D.B.V., and D.M.W. designed research; K.R.K., R.B., P.E.Z.L., and D.M.W. performed research; K.R.K. and D.M.W. contributed new reagents/analytic tools; K.R.K. and D.M.W. analyzed data; and K.R.K. and D.M.W. wrote the paper.

The authors declare no conflict of interest.

This article is a PNAS Direct Submission. A.J. is a guest editor invited by the Editorial Board.

Freely available online through the PNAS open access option.

[1]To whom correspondence should be addressed. E-mail: david.m.wilson@ucsf.edu.

This article contains supporting information online at www.pnas.org/lookup/suppl/doi:10.1073/pnas.1106920108/-/DCSupplemental.

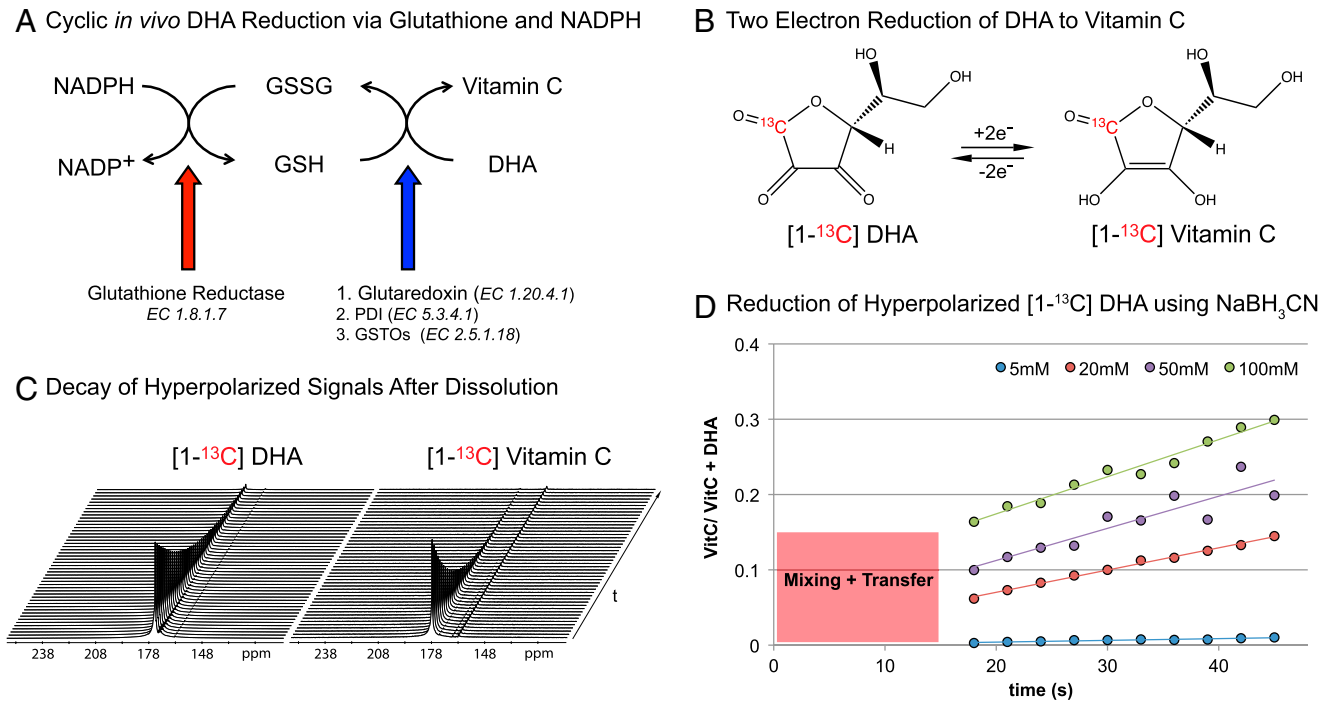

Fig. 1. Biochemical mechanism, hyperpolarization, and reduction of [1-^{13}C] DHA. (*A*) Relationship between redox pairs NADPH/NADP, GSSG/GSH and Vitamin C/DHA with associated enzymes. (*B*) Reversible reduction of labeled DHA to Vitamin C demonstrating the position of the hyperpolarized carbon. (*C*) Representative decays of hyperpolarized [1-^{13}C] DHA and [1-^{13}C] Vitamin C at 3 T. Spectra were acquired using a 5 ° pulse with 3 s temporal resolution. (*D*) Hyperpolarized [1-^{13}C] DHA (2.5 mM in water) was reacted with increasing concentrations of $NaBH_3CN$. A delay is included for mixing of the substrate with reducing agent and transfer to the magnet (15 s). VitC – VitaminC. VitC/[VitC + DHA] – Ratio of Vitamin C to sum of Vitamin C and DHA resonances.

Results

Synthesis, Polarization, and In Vitro Reduction of [1-^{13}C] DHA. In vitro methods to interrogate redox chemistry have relied on designer redox-sensitive fluorescent proteins (yellow- or green fluorescent protein) incorporating an artificial dithiol-disulfide pair (28), or on detection of ROS themselves via chemical switching (29). In general, fluorescent probes have limited clinical translation given poor tissue penetration; making MR-compatible hyperpolarized ^{13}C probes an attractive alternative. The technique is generally limited to endogenous biomolecules, given the relatively high concentrations of metabolic probes injected. Because the hyperpolarized ^{13}C signal can only be observed 1–2 min in vivo, rapid uptake and metabolism is an additional important requirement. The redox probe [1-^{13}C] DHA was designed with these general requirements in mind, minimizing T_1-dependent signal loss due to dipolar relaxation, and having sufficient chemical shift separation from [1-^{13}C] Vitamin C for in vivo MRSI. [1-^{13}C] DHA was prepared as a pure dimer by air oxidation of [1-^{13}C] ascorbic acid in the presence of catalytic amounts of copper (II) acetate, according to a published procedure (Fig. S1) (30). The material was polarized by using a dynamic nuclear polarization (DNP) approach (24) and dissolved with a hot water/ EDTA solution, with T_1's calculated as previously described (31). T_1's for the C_1 [1-^{13}C] DHA and [1-^{13}C] Vitamin C carbons are tabulated at both 11.7 T and 3 T, with the longest recorded T_1 that of [1-^{13}C] DHA at 3 T, 57 s (Fig. 1*C*, Table 1). There is a significant decrease in T_1 of the carbon of interest with increasing field strength. Due to chemical shift anisotropy, carbonyl carbons tend to decrease in T_1, leading to faster polarization decay with higher field strengths (32). The polarizations for [1-^{13}C] DHA and [1-^{13}C] Vitamin C were measured as 5.9 ± 0.5% and 3.6 ± 0.1% respectively, representing signal enhancements on the order of approximately 24,000- and 15,000-fold relative to thermal equilibrium at 3 T.

We next turned to a set of in vitro experiments to demonstrate (1) that we could reduce hyperpolarized [1-^{13}C] DHA using a water-soluble reducing agent (2) that the product [hyperpolarized [1-^{13}C]Vitamin C (VitC)] could be identified by chemical shift and (3) that the rate of this reaction depended on the concentration of the reducing agent. The reaction of hyperpolarized [1-^{13}C] DHA with $NaBH_3CN$ yields the reduced [1-^{13}C] Vitamin C within seconds, as described in Fig. 1*D*. Due to the higher stability of the DHA lactone at lower pH, these experiments were conducted in unbuffered solution at 37 °C, with a resulting pH of 4.5–5.5 (a slight pH increase was observed for increasing concentrations of $NaBH_3CN$). The equilibrium NMR spectrum of the purified dimeric [1-^{13}C] DHA demonstrated a single peak at 174 ppm. Following polarization, dissolution, and reaction with $NaBH_3CN$ a more complex spectrum was obtained, with evidence of rapid formation of [1-^{13}C] Vitamin C. On increasing concentrations of $NaBH_3CN$, enhanced rates of conversion to [1-^{13}C] Vitamin C were observed indicating dependence on the concentration of the reducing agent. Spectra at thermal equilibrium (without DNP)

Table 1. Chemical shifts, T_1 spin-lattice relaxation constants, solid-state build-up constants and percent polarization for [1-^{13}C] DHA and [1-^{13}C] VitC

	δ (ppm)	3 T T_1 (s)	11.7 T $T1$ (s)	Buildup constant (s)	Percent polarization
[1-^{13}C] DHA	174.0	56.5 ± 7.6	20.5 ± 0.9	1,120 ± 50	5.9 ± 0.5
[1-^{13}C] Vitamin C	177.8	29.2 ± 2.5	16.0 ± 0.8	1,756 ± 97	3.6 ± 0.1

Chemical shifts are relative to ^{13}C-urea at 163 ppm. For [1-^{13}C] DHA, measurements were performed in water at 37 °C (pH 4.5), while for [1-^{13}C] VitC measurements were performed in 100 mM phosphate buffer (pH 7.0). All measurements are reported as mean ± standard deviation.

were acquired immediately following these studies, and demonstrated only a single peak corresponding to [1-^{13}C] Vitamin C, confirmed by chemical shift, indicating that the reaction had gone to completion (Fig. S2).

Time-Resolved Magnetic Resonance Spectroscopy Confirms Rapid Reduction of Hyperpolarized [1-^{13}C] DHA In Vivo. Having demonstrated rapid reduction of hyperpolarized [1-^{13}C] DHA by a water-soluble reducing agent, we then turned to evidence of in vivo transformation. The transport of DHA in vivo occurs by a mechanism analogous to that of glucose, by facilitated diffusion using GLUT1, GLUT3, and GLUT4. Because glucose is known to compete with the uptake of DHA, in vivo experiments were performed on animals (mice and rats) fasted overnight. Animals were also pretreated with a DHA dose identical to that administered during the imaging experiment, 1 h prior which has been shown to reduce the physiologic effects of DHA administration (33). Time-resolved MRSI studies were carried out as previously published (26, 34). 350 μL of a hyperpolarized 15 mM [1-^{13}C] DHA solution were injected similar to previously described methods for [1-^{13}C] pyruvate, in normal mice with a ^{13}C urea phantom present for chemical shift reference. In a separate set of normal mice, similar experiments were performed using hyperpolarized [1-^{13}C] Vitamin C at a slightly higher concentration, 50 mM. Fig. 2 demonstrates the metabolism following injection of 15 mM hyperpolarized [1-^{13}C] DHA in a normal mouse. The DHA resonance at 174 ppm reached a maximum at 19 ± 1.7 s post injection. A large metabolite resonance was observed at 177.8 ppm, reaching a maximum at 29 ± 1.7 s, consistent with conversion to [1-^{13}C] Vitamin C in vivo. This chemical shift was confirmed both in vitro at neutral pH using ^{13}C urea as a reference, as well as in vivo with hyperpolarized [1-^{13}C] Vitamin C itself injected in a separate animal. For the latter experiment, trace oxidation to [1-^{13}C] DHA was observed in vivo (Fig. S3). These results are concordant with the literature regarding the bioconversion and uptake of DHA, reflected in the relative steady-state concentrations of DHA and Vitamin C in cells (35).

Reduction of Hyperpolarized [1-^{13}C] DHA In Vivo Localizes to Kidneys, Liver, Brain, and Tumor. In vivo reduction of hyperpolarized [1-^{13}C] DHA was expected to be fastest in tissues with high concentrations of GSH, namely the liver, kidneys, and lungs. In addition, we anticipated a contribution from highly glycolytic tissues, given the rapid transport properties of dehydroascorbate. Analogous to experiments performed previously using hyperpolarized [1-^{13}C] pyruvate, three-dimensional (3D) MRSI studies were conducted on a series of normal mice ($n = 5$) and TRAMP mice ($n = 4$), using a dual-tuned radio frequency (RF) coil (26), with 6 mm isotropic resolution. Nearly identical studies were performed in the rat brain ($n = 3$) with 5 mm isotropic resolution. Fig. 3 depicts characteristic 3D MRSI data obtained for TRAMP and normal mice, with the relative rates of [1-^{13}C] DHA reduction indicated by the magnitude of ^{13}C DHA and VitC resonances observed in different voxels. Sequential coronal T_2-weighted images and overlayed ^{13}C 3D MRSI for a TRAMP mouse are shown in Fig. 3 *A* and *B*, with regions of liver, kidney, and prostate tumor segmented and superimposed on the spectral grid. The liver and kidneys are best seen in the first image but present in both. Hyperpolarized ^{13}C spectra corresponding to tumor are seen in both Fig. 3 *A* and *B*, due to partial volume effects observed at this spatial resolution. Fig. 3*C* shows representative spectra obtained from different anatomic locations including tumor, while Fig. 3*D* depicts the normal mouse prostate gland in the axial plane with a representative ^{13}C spectrum, demonstrating no observable ^{13}C VitC. Fig. 3*E* summarizes the average metabolite ratios calculated for liver, kidney, normal prostate, TRAMP tumor, and voxels surrounding tumor in TRAMP mice. In normal mice, large Vitamin C resonances were observed in the murine liver (average VitC/[VitC + DHA] of 0.41 ± 0.03) and kidney (average VitC/[VitC + DHA] of 0.25 ± 0.03), and were significantly different ($p < 0.01$). These ratios did not vary significantly from those observed in TRAMP mice (average VitC/[VitC + DHA] of 0.44 ± 0.05 for the liver and 0.28 ± 0.01 for the kidney, $p = 0.61$ and 0.49 respectively). In tumors of TRAMP mice VitC/[VitC + DHA] averaged 0.23 ± 0.03, while significantly less Vitamin C signal was observed in the normal mouse prostate gland (VitC/[VitC + DHA] $= 0.06 \pm 0.03$, $p = 0.02$). Finally, conversion rates in TRAMP tumors were compared with those in surrounding voxels (caudal to the level of the kidneys and liver) for which the average VitC/[VitC + DHA] was 0.06 ± 0.02, significantly lower ($p < 0.01$). For a given TRAMP mouse, the average VitC/[VitC + DHA] ratio was 6.6-fold higher in tumor than in surrounding tissue. These data are summarized in Fig. 3*E*. Hyperpolarized ^{13}C MRSI data acquired from rat brains demonstrated an even greater ratio of VitC/[VitC + DHA] of 0.51 ± 0.1 with Vitamin C localized to the brain while DHA was present in the surrounding muscle tissue (Fig. 4).

Discussion

Alterations in cellular redox are implicated in a large number of pathologic processes, with a growing body of evidence also suggesting that controlled ROS chemistry is essential for normal

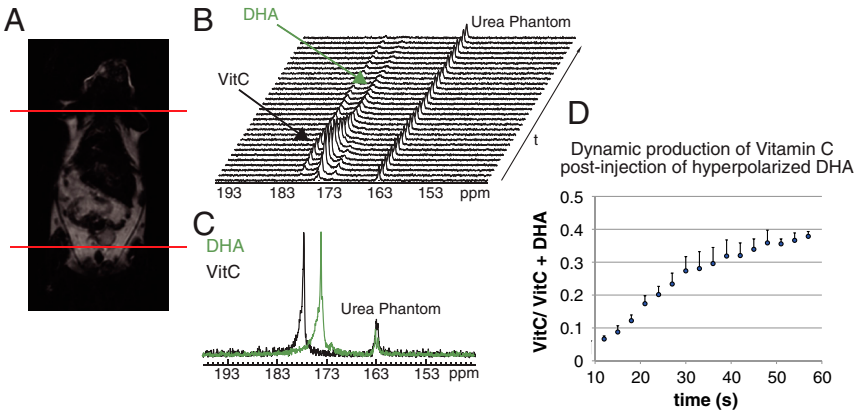

Fig. 2. Time-resolved ^{13}C spectra demonstrating the in vivo reduction of DHA to Vitamin C (*A*) Coronal T_2-weighted image of a normal mouse demonstrating the region of excitation for dynamic experiments. (*B*) Representative time-resolved spectra postinjection of 350 uL of 15 mM hyperpolarized [1-^{13}C] DHA. In vivo spectra were acquired using a 5 ° pulse with 3 s temporal resolution at 3 T. An 8 M ^{13}C-urea phantom was used as a chemical shift reference. (*C*) Spectra of each individual compound demonstrating the peak locations of DHA and Vitamin C (VitC) as compared to the dynamic data. (*D*) Average production of hyperpolarized Vitamin C in the dynamic spectra of normal mice ($n = 3$). Error bars indicate ± standard deviation of mean. VitC – VitaminC. VitC/[VitC + DHA] – Ratio of Vitamin C to sum of Vitamin C and DHA resonances.

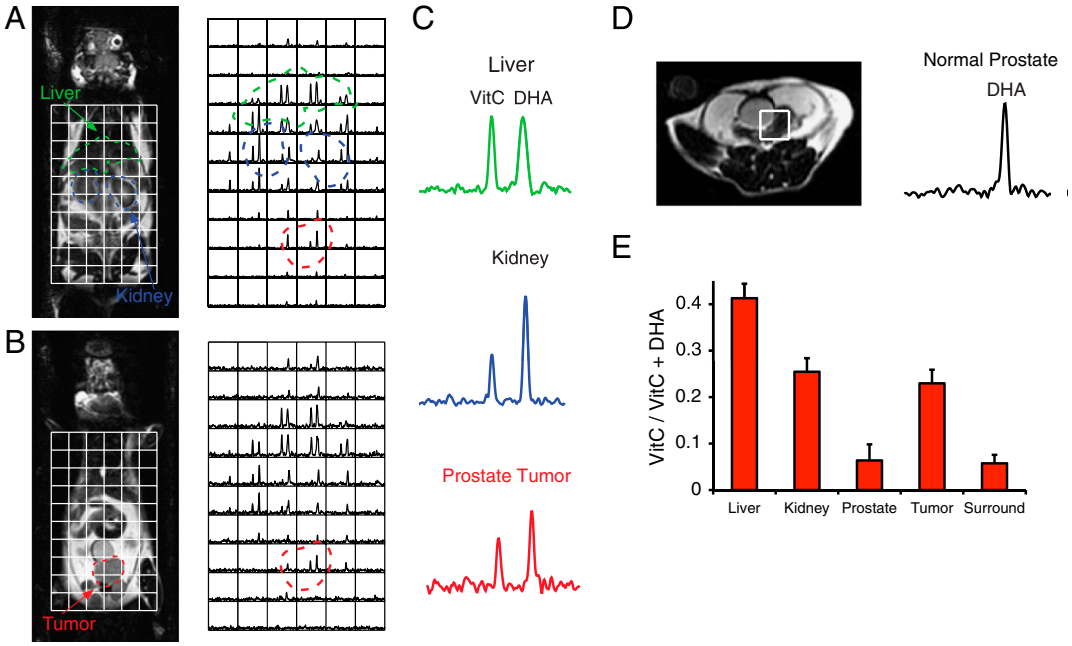

Fig. 3. (*A*, *B*) Sequential coronal T_2-weighted images and corresponding ^{13}C 3D MRSI demonstrating distribution of hyperpolarized DHA and Vitamin C (VitC) in a TRAMP mouse post intravenous injection of 350 uL of 15 mM hyperpolarized [1-^{13}C] DHA. This dataset was collected using a variable tip-angle scheme initiated 25 s following this injection, with individual voxels describing the relative reduction of [1-^{13}C] DHA to [1-^{13}C] VitC at the same time point. The liver and kidneys are best seen in (*A*) and prostate tumor in (*B*), but both imaging slices contain significant amounts of liver, kidney, and tumor tissue. Regions of liver, kidney, and prostate tumor are segmented and superimposed on the spectral grid (color-coded dashed lines). Differences in metabolite ratios are seen between normal organs and between prostate tumor and normal surrounding tissues. (*C*) Representative ^{13}C spectra from liver, kidney, and prostate tumor in a TRAMP mouse (*D*) Axial T_2-weighted image of a normal mouse with a voxel encompassing the normal prostate. (*E*) Summary of average metabolite ratios (VitC/[VitC + DHA]) for normal liver, kidneys, and prostate ($n = 5$), as well as TRAMP tumor and surrounding benign tissue (surround), ($n = 4$). All values are reported as mean ± standard error of the mean.

development (29). Given the universality of redox chemistry in the functional cell, we developed hyperpolarized [1-^{13}C] DHA, a MR-compatible endogenous probe to interrogate populations of key redox pairs in vivo, in particular GSH/ GSSG that are coupled to intracellular DHA reduction. The principal advantage of hyperpolarized ^{13}C MRI over other molecular imaging modalities is detection of ^{13}C metabolites by chemical shift, allowing real-time evaluation of physiologically relevant enzyme fluxes in vivo. Data obtained are potentially confounded by differential perfusion of (and transport into) tissues of interest, a problem that has been addressed by copolarization of ^{13}C probes with a perfusion agent, for example the intravascular agent ^{13}C urea (36). As for prior studies employing [1-^{13}C] pyruvate, we found for [1-^{13}C] DHA that the observed total ^{13}C signal (VitC+ DHA) was highest in tissues that are well perfused, including brain, liver, kidneys, and tumor. Although perfusion accounts for increased total ^{13}C signal in these tissues, we believe that the in vivo reduction of hyperpolarized [1-^{13}C] DHA is related both to its rapid transport into highly glycolytic cells, and the concentrations of key redox components within the cell, in particular GSH. Hyperpolarized [1-^{13}C] DHA was reduced rapidly to Vitamin C within the liver, as might be expected given both its high perfusion and role in GSH-dependent detoxification of electrophilic substances. To a lesser extent, the [1-^{13}C] Vitamin C metabolite was observed within kidneys and TRAMP tumors, the latter demonstrating both elevated glycolysis and high concentrations of GSH (37). Comparisons between TRAMP tumors and the normal murine prostate, as well as between TRAMP tumors and surrounding benign tissues indicated profound differences in ^{13}C DHA reduction that may be exploited in the detection and characterization of cancer.

For our ^{13}C 3D MRSI studies, we were able to obtain 6 mm isotropic resolution, in this case limited by signal to noise ratio (SNR). In the future, we anticipate improving anatomic resolution by (*i*) enhanced sensitivity through localized coils (up to 10-fold increase in SNR) (38–40); (*ii*) improved polarization methods, which include optimizing solvent, radical, and gadolinium-chelate (a potential fourfold increase in SNR if we obtain polarization similar to that of [1-^{13}C] pyruvate) (41); and (*iii*) MR techniques including more efficient sampling of k-space in order to reduce losses from T_1 and T_2 relaxation (42, 43). The advantages of better coil design are highlighted by the development of the endorectal coil that is the current standard for MR imaging of the prostate (40, 44), and murine brain studies in particular would benefit from dedicated head coils. These improvements in polarization and acquisition techniques would significantly improve the spatial resolution obtained, reducing partial volume effects and allowing a more detailed evaluation of specific tissues.

The steady-state concentration of Vitamin C in the brain is remarkably high, estimated to be 10 mM in neurons, while glia harbor high concentrations of GSH (45). This high Vitamin C level is generally attributed to the high rate of oxidative metabolism in neurons, making the brain particularly vulnerable to ROS and ischemia/reperfusion injury. Total brain Vitamin C levels are under strong homeostatic regulation, with extracellular Vitamin C concentrations mediated in part by heteroexchange with glutamate (46). High levels of brain Vitamin C are neuroprotective, and may be enhanced by administration of DHA, which readily

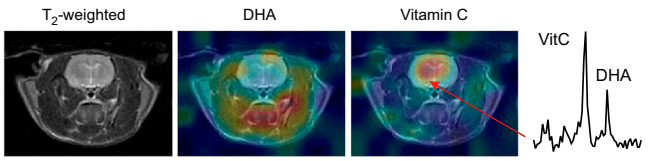

Fig. 4. Axial T_2-weighted images and corresponding color overlays of hyperpolarized DHA and Vitamin C (VitC) signal in a normal rat brain.

crosses the blood-brain barrier (47). On injection of hyperpolarized [1-^{13}C] DHA into a normal rat, significant reduction to [1-^{13}C] Vitamin C was observed within the brain, with essentially no background conversion observed in surrounding tissues. Given the limited spatial resolution of this study, we were not able to determine whether this reduction took place primarily in gray matter (dominated by neurons) or white matter (predominantly glia). Rapid reduction of hyperpolarized [1-^{13}C] DHA within the brain suggests a role for this probe in functional imaging (GLUT transporter density), determining local glutamate concentrations, as well as predicting vulnerability to ROS. More broadly, we anticipate many new applications of this MR probe to investigate the basic chemistry of living systems.

Materials and Methods

Synthesis of [1-^{13}C] DHA. [1-^{13}C] DHA (Isotec, Miamisburg, OH) was synthesized using a published method (Fig. S1), by air oxidation of [1-^{13}C] ascorbic acid in the presence of catalytic amounts of copper (II) acetate (30).

Hyperpolarization and Dissolution of [1-^{13}C] DHA and [1-^{13}C] Vitamin C. A 2.2 M solution of [1-^{13}C] DHA in dimethyacetamide (DMA) containing 15 mM OX063 trityl radical (48) (Oxford Instruments) was hyperpolarized on a HyperSense DNP instrument (Oxford Instruments) as previously described (34). The frozen sample was dissolved in distilled water containing 0.3 mM EDTA. Similarly, a 2.2 M solution of [1-^{13}C] Vitamin C (Omicron) was prepared as a sodium salt in NaOH/ water/ DMSO containing 15 mM OX063. This compound was polarized by an identical method and dissolved in 100 mM phosphate buffer, pH 7.0.

11.7 T NMR Studies. NMR studies were performed on an 11.7 T Varian INOVA spectrometer (125 MHz ^{13}C, Varian Instruments) using a 10 mm ^{15}N/^{31}P/^{13}C broadband direct detect probe. Time-resolved hyperpolarized spectra, as well as spectra at thermal equilibrium were obtained for [1-^{13}C] DHA and [1-^{13}C] Vitamin C as previously described, and used to calculate T_1's and signal enhancements (34). For NMR studies of the reduction of [1-^{13}C] DHA to [1-^{13}C] Vitamin C, hyperpolarized [1-^{13}C] DHA was reacted with an excess of sodium cyanoborohydride ($NaBH_3CN$). Following dissolution of hyperpolarized [1-^{13}C] DHA in water containing 0.3 mM EDTA, $NaBH_3CN$ in water was added and the resulting solution rapidly mixed in a 10 mm NMR tube. In each case the final concentration of DHA was 2.5 mM while the $NaBH_3CN$ concentration range was 5–100 mM, resulting in a measured pH of 4.5–5.5. The mixing and transfer time was 15 s in each case. As for T_1 measurements, time-resolved spectra were obtained every 3 s using a 5 ° pulse.

3 T Studies. T_1 studies were performed using a 3 T MRI scanner (GE Healthcare) equipped with the MNS (multinuclear spectroscopy) hardware package. The RF coil used in these experiments was a dual-tuned ^{1}H-^{13}C coil with a quadrature ^{13}C channel and linear ^{1}H channel construction used in ^{13}C mouse imaging studies (26). Prior to ^{13}C studies, 3-plane T_2-weighted images were acquired for anatomic localization ($T_E = 100$ ms, $T_R = 4$ s, 6 averages) using a standard fast spin echo sequence. ^{13}C MRSI studies were carried out as previously published (26). 350 μL (mice) or 2 mL (rats) of a hyperpolarized 15 mM [1-^{13}C] DHA solution were injected similar to previously described methods for [1-^{13}C] pyruvate. For all imaging experiments, an 8 M ^{13}C urea phantom in a sealed tube was placed within the sensitive volume of the RF coil. Similar experiments were performed on a set of normal mice using hyperpolarized [1-^{13}C] Vitamin C at 50 mM. For the in vivo dynamic experiments, the first spectrum was obtained 3 s after starting the ^{13}C agent injection, and every 3 s thereafter. For the ^{13}C 3D MRSI studies, the imaging sequence was initiated 10 s following completion of a 15 s injection (representing a total delay of 25 s). Time-resolved ^{13}C spectra were acquired using a five-degree excitation while the ^{13}C 3D MRSI used a variable flip angle scheme, matrix size of $8 \times 8 \times 16$ and voxel size of 6 mm isotropic.

Data Processing and Analysis. All solution data was processed using ACD Labs NMR Processor (ACD Labs). In vivo MRSI data was processed using custom software written in IDL 8 (ITT Visual Information Solutions) and Matlab 2009b (MathWorks). DHA and Vitamin C resonances were integrated and peak heights were used to calculate relevant ratios. In order to assign voxels to a given tissue type, >70% of a given voxel corresponded to the tissue of interest as validated by the corresponding T_2-weighted image. Average metabolite ratios (VitC/[VitC + DHA]) for liver, kidney, and normal prostate were calculated from normal mice ($n = 5$), while TRAMP mice ($n = 4$) were used to calculate metabolite ratios for tumor and surrounding benign tissues. The average number of voxels (per animal) used to determine the VitC/[VitC + DHA] ratio in a given tissue were as follows: liver 5.1 ± 0.3, kidney 7.1 ± 0.7, prostate 3.0 ± 0.6, tumor 12.5 ± 2.0, and surrounding tissues 11.3 ± 1.5. The number of tumor voxels (and surrounding tissues) used varied with tumor size (ranging from 1 to 4 cc).

ACKNOWLEDGMENTS. Grant sponsors National Institutes of Health (R21 EB005363, R01 EB007588, R00 EB012064, P41 EB013598).

1. Murad S, et al. (1981) Regulation of collagen synthesis by ascorbic acid. *Proc Natl Acad Sci USA* 78:2879–2882.
2. Tolbert LC, Thomas TN, Middaugh LD, Zemp JW (1979) Effect of ascorbic acid on neurochemical, behavioral, and physiological systems mediated by catecholamines. *Life Sci* 25:2189–2195.
3. Glembotski CC (1987) The role of ascorbic acid in the biosynthesis of the neuroendocrine peptides alpha-MSH and TRH. *Ann NY Acad Sci* 498:54–62.
4. Kojo S (2004) Vitamin C: basic metabolism and its function as an index of oxidative stress. *Curr Med Chem* 11:1041–1064.
5. Bergsten P, et al. (1990) Millimolar concentrations of ascorbic acid in purified human mononuclear leukocytes. Depletion and reaccumulation. *J Biol Chem* 265:2584–2587.
6. Anderson R, Stankova L, Bigley RH, Bagby GC, Jr (1983) Dehydroascorbate uptake as an in vitro biochemical marker of granulocyte differentiation. *Cancer Res* 43:4696–4698.
7. Washko P, Rotrosen D, Levine M (1989) Ascorbic acid transport and accumulation in human neutrophils. *J Biol Chem* 264:18996–19002.
8. Wells WW, Xu DP (1994) Dehydroascorbate reduction. *J Bioenerg Biomembr* 26:369–377.
9. Linster CL, Van Schaftingen E (2007) Vitamin C. Biosynthesis, recycling and degradation in mammals. *FEBS J* 274:1–22.
10. Del Bello B, et al. (1994) Purification of NADPH-dependent dehydroascorbate reductase from rat liver and its identification with 3 alpha-hydroxysteroid dehydrogenase. *Biochem J* 304:385–390.
11. Whitbread AK, et al. (2005) Characterization of the omega class of glutathione transferases. *Methods Enzymol* 401:78–99.
12. Maellaro E, et al. (1994) Purification and characterization of glutathione-dependent dehydroascorbate reductase from rat liver. *Biochem J* 301:471–476.
13. Kosower NS, Kosower EM (1978) The glutathione status of cells. *Int Rev Cytol* 54:109–160.
14. Cartwright RA, et al. (1982) Role of N-acetyltransferase phenotypes in bladder carcinogenesis: a pharmacogenetic epidemiological approach to bladder cancer. *Lancet* 2:842–845.
15. Nakajima T, et al. (1995) Expression and polymorphism of glutathione S-transferase in human lungs: risk factors in smoking-related lung cancer. *Carcinogenesis* 16:707–711.
16. Balendiran GK, Dabur R, Fraser D (2004) The role of glutathione in cancer. *Cell Biochem Funct* 22:343–352.
17. Midander J, Deschavanne PJ, Malaise EP, Revesz L (1982) Survival curves of irradiated glutathione-deficient human fibroblasts: indication of a reduced enhancement of radiosensitivity by oxygen and misonidazole. *Int J Radiat Oncol Biol Phys* 8:443–446.
18. Nguyen LN, Munshi A, Hobbs ML, Story MD, Meyn RD (2001) Paclitaxel restores radiation-induced apoptosis in a bcl-2-expressing, radiation-resistant lymphoma cell line. *Int J Radiat Oncol Biol Phys* 49:1127–1132.
19. Halliwell B (1994) Free radicals, antioxidants, and human disease: curiosity, cause, or consequence? *Lancet* 344:721–724.
20. Choy G, Choyke P, Libutti SK (2003) Current advances in molecular imaging: noninvasive in vivo bioluminescent and fluorescent optical imaging in cancer research. *Mol Imaging* 2:303–312.
21. Thelwall PE, et al. (2005) Noninvasive in vivo detection of glutathione metabolism in tumors. *Cancer Res* 65:10149–10153.
22. Liang WJ, Johnson D, Jarvis SM (2001) Vitamin C transport systems of mammalian cells. *Mol Membr Biol* 18:87–95.
23. Kurhanewicz J, et al. (2011) Analysis of cancer metabolism by imaging hyperpolarized nuclei: prospects for translation to clinical research. *Neoplasia* 13:81–97.
24. Ardenkjaer-Larsen JH, et al. (2003) Increase in signal-to-noise ratio of >10,000 times in liquid-state NMR. *Proc Natl Acad Sci USA* 100:10158–10163.
25. Golman K, Ardenkjaer-Larsen JH, Petersson JS, Mansson S, Leunbach I (2003) Molecular imaging with endogenous substances. *Proc Natl Acad Sci USA* 100:10435–10439.
26. Kohler SJ, et al. (2007) In vivo 13 carbon metabolic imaging at 3T with hyperpolarized 13C-1-pyruvate. *Magn Reson Med* 58:65–69.
27. Larson PE, et al. (2011) Fast dynamic 3D MR spectroscopic imaging with compressed sensing and multiband excitation pulses for hyperpolarized 13C studies. *Magn Reson Med* 65:610–619.
28. Gutscher M, et al. (2008) Real-time imaging of the intracellular glutathione redox potential. *Nat Methods* 5:553–559.
29. Dickinson BC, Peltier J, Stone D, Schaffer DV, Chang CJ (2011) Nox2 redox signaling maintains essential cell populations in the brain. *Nat Chem Biol* 7:106–112.
30. Koliou EK, Ioannou PV (2005) Preparation of dehydro-L-ascorbic acid dimer by air oxidation of L-ascorbic acid in the presence of catalytic amounts of copper(II) acetate and pyridine. *Carbohydr Res* 340:315–318.
31. Wilson DM, et al. (2009) Generation of hyperpolarized substrates by secondary labeling with [1,1-13C] acetic anhydride. *Proc Natl Acad Sci USA* 106:5503–5507.

32. Blicharski JS (1972) Nuclear magnetic relaxation by anisotropy of the chemical shift. *Z Naturforsch Pt A* 27:1456–1458.
33. Patterson JW, Mastin DW (1951) Some effects of dehydroascorbic acid on the central nervous system. *Am J Physiol* 167:119–126.
34. Keshari KR, et al. (2009) Hyperpolarized [2-13C]-fructose: a hemiketal DNP substrate for in vivo metabolic imaging. *J Am Chem Soc* 131:17591–17596.
35. May JM, Qu ZC, Neel DR, Li X (2003) Recycling of vitamin C from its oxidized forms by human endothelial cells. *Biochim Biophys Acta* 1640:153–161.
36. Wilson DM, et al. (2010) Multi-compound polarization by DNP allows simultaneous assessment of multiple enzymatic activities in vivo. *J Magn Reson* 205:141–147.
37. Raina K, Serkova NJ, Agarwal R (2009) Silibinin feeding alters the metabolic profile in TRAMP prostatic tumors: 1H-NMRS-based metabolomics study. *Cancer Res* 69:3731–3735.
38. Hoult DI, Lauterbur PC (1979) Sensitivity of the Zeugmatographic experiment involving human samples. *J Magn Reson* 34:425–433.
39. Roemer PB, Edelstein WA, Hayes CE, Souza SP, Mueller OM (1990) The Nmr Phased-Array. *Magnet Reson Med* 16:192–225.
40. Hricak H, et al. (1994) Carcinoma of the prostate gland: MR imaging with pelvic phased-array coils versus integrated endorectal–pelvic phased-array coils. *Radiology* 193:703–709.
41. von Morze C, et al. (2011) Multi-band frequency encoding method for metabolic imaging with hyperpolarized [1-(13)C]pyruvate. *J Magn Reson* 211:109–113.
42. Cunningham CH, et al. (2008) Pulse sequence for dynamic volumetric imaging of hyperpolarized metabolic products. *J Magn Reson* 193:139–146.
43. Leupold J, Mansson S, Petersson JS, Hennig J, Wieben O (2009) Fast multiecho balanced SSFP metabolite mapping of (1)H and hyperpolarized (13)C compounds. *Magnetic Resonance Materials in Physics, Biology and Medicine (MAGMA)* 22:251–256.
44. Schnall MD, Lenkinski RE, Pollack HM, Imai Y, Kressel HY (1989) Prostate: MR imaging with an endorectal surface coil. *Radiology* 172:570–574.
45. Rice ME, Russo-Menna I (1998) Differential compartmentalization of brain ascorbate and glutathione between neurons and glia. *Neuroscience* 82:1213–1223.
46. Rebec GV, Pierce RC (1994) A vitamin as neuromodulator: ascorbate release into the extracellular fluid of the brain regulates dopaminergic and glutamatergic transmission. *Prog Neurobiol* 43:537–565.
47. Huang J, et al. (2001) Dehydroascorbic acid, a blood-brain barrier transportable form of vitamin C, mediates potent cerebroprotection in experimental stroke. *Proc Natl Acad Sci USA* 98:11720–11724.
48. Reddy TJ, Iwama T, Halpern HJ, Rawal VH (2002) General synthesis of persistent trityl radicals for EPR imaging of biological systems. *J Org Chem* 67:4635–4639.